Reactions of Methyl- and Ethylperoxy Radicals with NO Studied by Time-Resolved Negative Ionization Mass Spectrometry

Jia-Hua Xing, Yoko Nagai, Masayuki Kusuhara, and Akira Miyoshi*

Department of Chemical System Engineering, The University of Tokyo, 7-3-1 Hongo, Bunkyo-ku, Tokyo 113-8656 Japan

Received: May 7, 2004; In Final Form: August 23, 2004

The rate constants for the gas-phase reactions of methyl- and ethylperoxy radicals with NO were studied at room temperature (298 ± 2 K) and 4 Torr of pressure (He buffer) by using a laser flash photolysis coupled with time-resolved negative ionization mass spectrometry technique. The alkyl peroxy radicals were generated by the reaction of corresponding alkyl radicals with excess O_2, where alkyl radicals were prepared by laser photolysis of several precursor molecules. The rate constants were determined to be $k(CH_3O_2 + NO) = (9.9 \pm 2.1) \times 10^{-12}$ and $k(C_2H_5O_2 + NO) = (11.0 \pm 0.8) \times 10^{-12}$ cm^3 molecule^{-1} s^{-1} which are about a factor of 1.3 larger than the previous recommendations.

1. Introduction

Peroxy radicals play an important role in the atmospheric photooxidation processes. Organic peroxy radicals are generated in the degradation process of organic compounds released into the troposphere. Alkyl peroxy radicals (RO_2) are formed through the OH-initiated oxidation of alkanes (RH).[1]

$$RH + OH \rightarrow R + H_2O \quad (1)$$

$$R + O_2 + M \rightarrow RO_2 + M \quad (2)$$

Due to the low reactivity toward closed shell molecules, RO_2 radicals are mainly removed by the reactions with NO, HO_2, and other peroxy radicals. In the polluted air, with sufficient concentration of NO_x, RO_2 radicals react predominantly with NO.

$$RO_2 + NO \rightarrow RO + NO_2 \quad (3a)$$

$$RO_2 + NO + M \rightarrow RONO_2 + M \quad (3b)$$

Reaction 3a leads to the formation of ozone in the troposphere via

$$NO_2 + h\nu\ (\lambda < 380\ \text{nm}) \rightarrow NO + O \quad (4)$$

$$O + O_2 + M \rightarrow O_3 + M \quad (5)$$

Reaction 3b is pressure dependent, and acts as a temporal sink for both alkyl peroxy radicals and NO. The branching ratio, k_{3b}/k_{3a}, increases monotonically with the carbon number of the peroxy radical, and for the ethylperoxy radical it is reported to be ≤0.014 at tropospheric conditions, while that of methylperoxy radical is negligible.[2]

There have been numerous kinetic studies on the reaction of methylperoxy radical (CH_3O_2) with NO,[3−14] because methane is the most abundant organic compound in the troposphere. Also, several studies have been reported on the reaction of ethylperoxy radical with NO.[10,15−20] Two major experimental techniques applied in these previous studies are the (laser-)flash photolysis−UV absorption technique and the flow-tube−mass spectrometry technique. It has been well-known that the UV−absorption technique is easily suffered from the interference absorption of products and byproducts. Although the chemical ionization mass spectrometry has been reported to be a selective and sensitive technique, the ionization reaction requires a long reaction time and can only be combined with the flow-tube method. Masaki et al.[12] examined the reaction $CH_3O_2 + NO$ by using laser photolysis−photoionization mass spectrometry, which was innovative in applying the selective detection method in the time-resolved measurement of methylperoxy radicals for the first time. Unfortunately, this method is not applicable to other alkyl peroxy radicals with larger alkyl groups. Although no significant flaw could be found either in their or the other previous measurements, their rate constant was significantly larger than previous studies. To resolve the discrepancy, other experimental studies, preferably with different experimental technique, are desirable.

In this study, a new method for kinetics measurements of peroxy radicals, negative ionization mass spectrometry, has been developed. In general, peroxy radicals are expected to have positive electron affinity, that is, the anions of peroxy radicals will be stable. Several previous studies were successful in detecting the ethyl peroxy radical by chemical negative ionization.[15,19]

This article reports the investigation on the kinetics of the following reactions conducted at room temperature (298 ± 2 K) and at a total pressure of 4 Torr of He.

$$CH_3O_2 + NO \rightarrow CH_3O + NO_2 \quad (6)$$

$$C_2H_5O_2 + NO \rightarrow C_2H_5O + NO_2 \quad (7)$$

2. Experimental Section

Laser Flash Photolysis−Negative Ionization Mass Spectrometry. A schematic of the experimental apparatus is shown

* Address correspondence to this author. E-mail: miyoshi@chemsys.t.u-tokyo.ac.jp.

10.1021/jp0480347 CCC: $27.50
Published on Web 10/29/2004

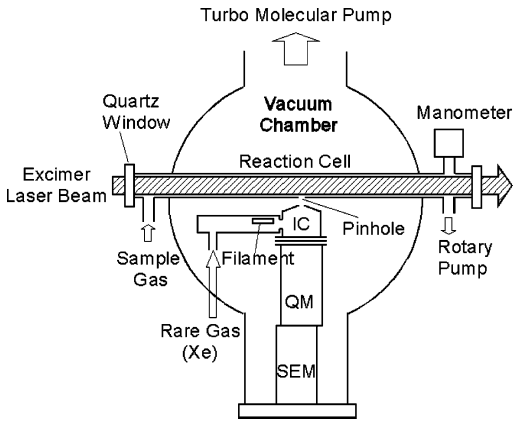

Figure 1. A schematic diagram of the laser flash photolysis−negative ionization mass spectrometry apparatus: IC, ionization chamber; QM, quadrupole mass filter; SEM, secondary electron multiplier.

in Figure 1. The reactant gas mixtures diluted in helium were flowed into a tubular Pyrex photolysis cell (85 cm in length and 16 mm in diameter) and irradiated by ArF (193 nm) or KrF (248 nm) excimer laser (Lambda Physik, Compex 102). The pressure was measured with a capacitance manometer (MKS Baratron Type 622). The reacting gases were sampled through a 200-μm pinhole, which was located on the wall of the reactor at a distance of 45 cm from the inlet port, and led into the ionization chamber. The evacuation port and the pressure-measurement port are located 40 cm downstream from the pinhole. The flow velocity in the reaction cell was kept high enough, $\sim$13 m s^{-1}, to ensure the complete replacement of gases between the laser shots fired with the repetition rate of 9−12 Hz.

Peroxy radicals were negatively ionized by the electron transfer from high-Rydberg state rare gas atoms (Rg**).

$$\mathrm{Rg^{**} + RO_2 \rightarrow Rg^+ + RO_2^-} \qquad (8)$$

The principle of the ionization method has been described by Kondow.[21] Because the RO_2 detection sensitivity was found to be the highest among the available rare gases, Ar, Kr, and Xe, xenon was used as the ionization rare gas atom in this study. A cross-sectional view of the ionization chamber is shown in Figure 2. Gaseous xenon was continuously introduced into a tube attached to the ionization chamber and was excited to high-Rydberg states (Xe**) by electron impact, using a helical filament made of thoria-coated tungsten. The gas pressure in the electron-impact tube was maintained at a few milliTorr. The electron energy was kept at 34 eV where the highest sensitivity was obtained. The emission current was 21 μA through all experiments. A grid electrode was placed between the electron-impact tube and the ionization chamber was kept at sufficiently minus voltage so that the electrons and anionic species could be repelled and the cationic species could be absorbed. Thus only the neutral species were introduced into the ionization chamber. The ionization chamber, which acts as an ion repeller electrode, was kept at −9 to −11 V from the ground, and the electron-impact tube was also kept −10 V from the ground. The confinement factor of the ionization chamber was optimized by adjusting the size of the three holes open to the main vacuum chamber. Since an apparent tradeoff relation was found between the detection sensitivity and the detection time resolution, near the lowest allowable time resolution, $\sim$2 ms, was chosen. The negatively ionized species were extracted by the first electrode of the ion-lens system kept at +8 V, collimated by the ion lens,

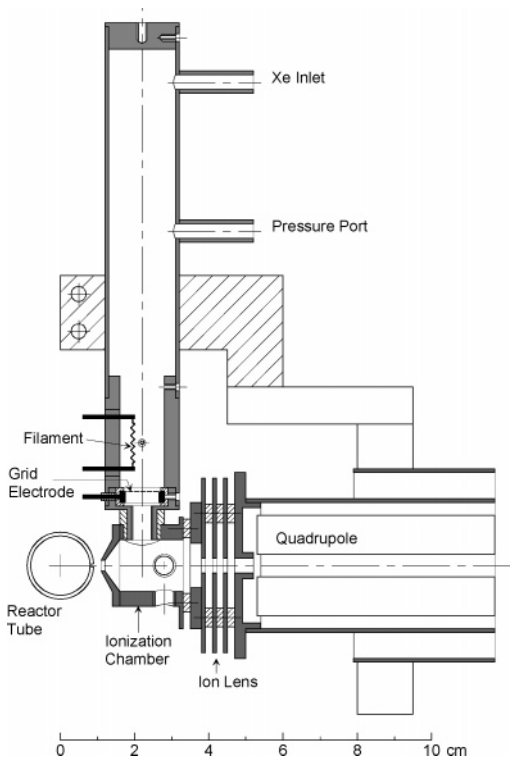

Figure 2. A cross-sectional view of the ionization chamber. See text for details.

and introduced into the quadrupole mass filter (Anelva AQA-360). The mass selected ion-beam was deflected and introduced to the first dynode (made of Cu−Be) of the SEM (secondary electron multiplier; Hamamatsu R515), which was placed off-axis of the quadrupole. Because the Cu−Be dynode is sensitive to the vacuum-ultraviolet light emitted from the electron-impact tube, the off-axis alignment was inevitable to reduce the background noise. Since, for the anion detection, the collector electrode of the SEM must be kept at a high voltage ($\sim$ 4 kV) from the ground, the ion current was amplified with a battery-operated I−V converter circuit and transmitted to the discriminator circuit via a photocoupler isolator. The ion signals were processed with a multichannel scaling circuit interfaced to a personal computer. The gate width was set at 50 or 100 μs. To obtain a temporal profile of the RO_2 concentration, the ion signals were accumulated over 10 000−20 000 laser shots.

Reactant Preparation. To examine the possible contribution of the secondary kinetics, several precursors were used for each alkyl peroxy radical. The alkyl peroxy radicals were generated by reacting either methyl radicals ($1.0-1.6 \times 10^{12}$ molecules cm^{-3}) or ethyl radicals ($4-12 \times 10^{12}$ molecules cm^{-3}) with excess O_2 in the He diluent gas of total 4 Torr pressure. The radical concentrations were kept low enough to avoid radical−radical reactions. Methyl radicals were produced either by 193-nm laser photolysis of acetone or by 248-nm laser photolysis of methyl iodide.

$$\mathrm{CH_3COCH_3} + h\nu\ (193\ \mathrm{nm}) \rightarrow 2\mathrm{CH_3} + \mathrm{CO} \qquad (9)$$

$$\mathrm{CH_3I} + h\nu\ (248\ \mathrm{nm}) \rightarrow \mathrm{CH_3} + \mathrm{I} \qquad (10)$$

Ethyl radicals were produced by three methods: 248-nm photolysis of ethyl iodide, 193-nm photolysis of ethyl bromide, and the reaction of Cl atoms with ethane in which CCl_4 was

subjected to 193-nm photolysis to produce Cl atoms.

$$C_2H_5I + h\nu\ (248\ nm) \rightarrow C_2H_5 + I \quad (11)$$

$$C_2H_5Br + h\nu\ (193\ nm) \rightarrow C_2H_5 + Br \quad (12)$$

$$CCl_4 + h\nu\ (193\ nm) \rightarrow Cl + CCl_3 \quad (13a)$$

$$\rightarrow 2Cl + CCl_2 \quad (13b)$$

$$Cl + C_2H_6 \rightarrow C_2H_5 + HCl \quad (14)$$

The concentration of O_2 was set to 2.0 and 0.6 Torr for the preparation of CH_3O_2 and $C_2H_5O_2$, respectively, such that the formation of RO_2 was completed within 0.1 ms. The NO concentration was varied within the range where the reaction of RO_2 + NO could be observed in a time scale of 3 to 25 ms. The oxidation of NO by the reaction of $2NO + O_2 \rightarrow 2NO_2$ was negligible in the experimental condition.

The following gases and reagents were used without further purification; helium (Nippon Sanso, 99.9999%), O_2 (Nippon Sanso, 99.99%), NO/He (Nippon Sanso, 5.48%), acetone (Tokyo Kasei, >99.5%), CH_3I (Wako Pure Chemical, >99.5%), C_2H_6 (Nippon Sanso, 99.9%), CCl_4 (Wako Pure Chemical, >99.8%), C_2H_5I (Tokyo Kasei, >99.0%), C_2H_5Br (Tokyo Kasei, >99%), acetone-d_6 (Wako Pure Chemica,l 99.9%). All the liquid samples were deaerated before use.

Experimental Conditions and Data Analysis. Kinetics measurement was carried out at a laser repetition of 9−12 Hz to ensure complete replenishment of the gas sample between successive laser shots. Temporal profiles of the ion signal were recorded from 20 ms before to 30 ms after the photolysis laser pulse. The fitting range in the analysis was from 3 to 15−25 ms after the laser photolysis depending on the decay time constant. Signals were accumulated over 10 000−20 000 laser shots to increase the signal-to-noise ratio. The laser fluence in the experiments was in the range 3−10 mJ cm^{-2} $pulse^{-1}$ for 193 nm and 16−37 mJ cm^{-2} $pulse^{-1}$ for 248 nm. The initial concentration of peroxy radicals was evaluated from the precursor concentration and the laser fluence with use of the following data. The absorption cross section (σ) and the photolysis quantum yield (Φ) of the precursors are as follows: acetone, $\sigma = 200 \times 10^{-20}$ cm^2, $\Phi_9 = 0.96$ at 193 nm;[22,23] CCl_4, $\sigma = 88.2 \times 10^{-20}$ cm^2, $\Phi(Cl) = 1.56$ at 193 nm;[24] CH_3I, $\sigma = 80.6 \times 10^{-20}$ cm^2, $\Phi(C_2H_5) \approx 1$ at 248 nm;[24] C_2H_5I, $\sigma = 83.7 \times 10^{-20}$ cm^2, $\Phi(C_2H_5) \approx 1$ at 248 nm;[25,26] C_2H_5Br, $\sigma = 44.6 \times 10^{-20}$ cm^2,[27] $\Phi(C_2H_5) = 0.82$ at 193 nm.[28] A large excess of molecular oxygen was added so that the conversion of alkyl radicals to the corresponding alkyl peroxy radicals was almost instantaneous compared to the time scale of the reaction of interest. Experiments were carried out at room temperature (298 ± 2 K) with a total pressure of 4 Torr of helium.

The detection limits of methyl- and ethylperoxy radicals at 1.0-s acquisition time were 3.2×10^{11} and 5.2×10^{11} molecules cm^{-3}, respectively. The rate constants for reactions 6 and 7, k_6 and k_7, were determined by detailed kinetic models with all considerable reactions occurring in the reaction systems using Chemkin-II.[29] The rate constants of side reactions were obtained from JPL Evaluation No. 14[25] or the IUPAC 2002 summary.[24]

3. Results and Discussion

Reaction of CH_3O_2 + NO. Figure 3 shows typical temporal profiles of the signal at *m/z* 47 ($CH_3O_2^-$). At first, a simple

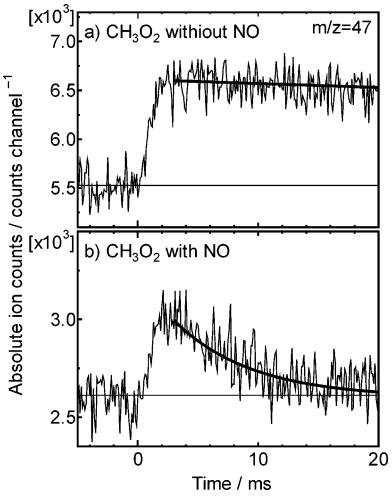

Figure 3. Typical temporal profiles of $CH_3O_2^-$ signals. Experimental conditions: $[CH_3O_2]_0 = 1.2 \times 10^{12}$ molecules cm^{-3}, total pressure = 4 Torr, and (a) [NO] = 0 and (b) 0.36 mTorr. The lines denote the results of single-exponential fitting.

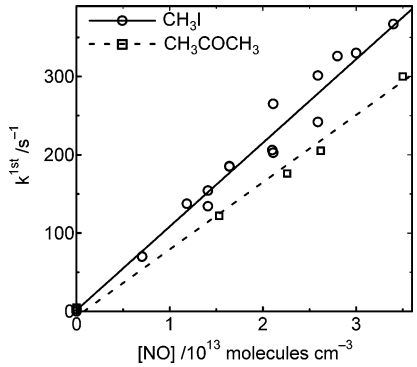

Figure 4. Plot of observed first-order rate constants (k^{1st}) versus NO concentration for the CH_3O_2 + NO reaction. The symbols denote experimental results with CH_3I (circles) and acetone (squares) as CH_3 precursor, respectively. The solid and dotted lines represent their least-squares fits to CH_3I data and acetone data, respectively. The smaller rate constant for acetone data is the result of regeneration of CH_3O_2 by the subsequent reactions (see text for details).

analysis assuming the pseudo-first-order condition

$$[CH_3O_2] = [CH_3O_2]_0 \exp(-k^{1st}t) \quad (E1)$$

$$k^{1st} = k_6[NO] + k_w \quad (E2)$$

was made. Here k_6 is the overall rate constant for the CH_3O_2 + NO reaction and k_w is that for other loss processes, mainly the wall loss process. Experimental k_w was ~3 s^{-1} for CH_3O_2. Due to the low concentration of peroxy radicals, the contribution of the radical−radical reaction, $CH_3O_2 + CH_3O_2$, was negligible as can be seen from Figure 3a. The experimental CH_3O_2 decay profiles were fitted to eq E1, and the values of k^{1st} were derived for several NO concentrations. First-order plots according to eq E2 are shown in Figure 4. When acetone was used as a precursor, k_6 was derived to be 8.3×10^{-12} cm^3 $molecule^{-1}$ s^{-1}, while it was 9.9×10^{-12} cm^3 $molecule^{-1}$ s^{-1} when CH_3I was used.

In the detailed analysis with the chemical model including the secondary reactions, it was recognized that the regeneration of methylperoxy radicals from secondary kinetics affects the measurements when acetone is used as a precursor. In contrast, secondary reactions are little affected when CH_3I was used as the precursor.

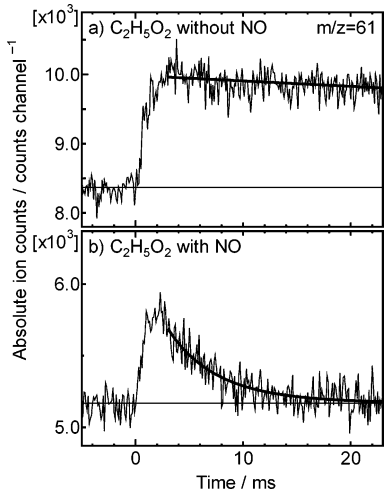

Figure 5. Typical temporal profiles of $C_2H_5O_2^-$ signals. Experimental conditions: $[C_2H_5O_2]_0 = 4.9 \times 10^{12}$ molecules cm^{-3}, total pressure = 4 Torr, and (a) [NO] = 0 and (b) 0.69 mTorr. The lines denote the results of (a) single-exponential fitting and (b) fitting to the second-order formula (see text for details).

In the acetone system, the regeneration of CH_3O_2 is initiated by the OH radicals produced in the following subsequent reactions:

$$CH_3O_2 + NO \rightarrow CH_3O + NO_2 \quad (6)$$

$$CH_3O + O_2 \rightarrow CH_2O + HO_2 \quad (15)$$

$$HO_2 + NO \rightarrow OH + NO_2 \quad (16)$$

$$CH_3COCH_3 + OH \rightarrow CH_3 + CH_3C(=O)OH \quad (17)$$

$$CH_3 + O_2 + M \rightarrow CH_3O_2 + M \quad (2a)$$

Numerical simulation for the acetone system with $k_6 = (9.9 \pm 2.1) \times 10^{-12}$ cm^3 molecule^{-1} s^{-1}, which is derived from the CH_3I experiment, successfully reproduces the experimental profiles.

Reaction of $C_2H_5O_2$ + NO. Typical observed temporal profiles of the signal at *m*/*z* 61 ($C_2H_5O_2^-$) are shown in Figure 5. Because of the inferior detection sensitivity of $C_2H_5O_2$ to that of CH_3O_2, the ratio, $[NO]/[C_2H_5O_2]$, was 2.5−6.2 and the pseudo-first-order condition could not be assumed. Therefore, the analyses were made by using the second-order formula:

$$[C_2H_5O_2] = \frac{\alpha}{\beta \exp(\alpha k_7 t) - 1}$$

$$\alpha = [NO]_0 - [C_2H_5O_2]_0; \beta = [NO]_0/[C_2H_5O_2]_0 \quad (E3)$$

where k_7 is the overall rate constant for the reaction of $C_2H_5O_2$ + NO. Examples of the observed $C_2H_5O_2$ decay profiles and the results of the fitting to eq E3 are shown in Figure 5b. The derived rate constant was 11.0×10^{-12} cm^3 molecule^{-1} s^{-1} in either experiment with C_2H_5I or C_2H_5Br as the C_2H_5 radical precursor as shown in Table 1. For the experiments with C_2H_6/CCl_4 as radical precursor, the derived rate constant was much smaller in the range of 5.8×10^{-12} to 4.2×10^{-12} cm^3 molecule^{-1} s^{-1}. A numerical analysis for $C_2H_6-CCl_4$ experiments including the side reactions showed the significant reproduction of $C_2H_5O_2$ via OH radical formed from the following reactions:

TABLE 1: Experimental Conditions and the Derived Rate Constant for $C_2H_5O_2$ + NO

$[C_2H_5I]_0$[b]	laser fluence[c] (248 nm)	$[C_2H_5O_2]_0$[a,d]	[NO][d]	k_7[e]
3.9	25.4	10.2	30.7	11.3
3.9	25.4	10.2	40.1	11.3
3.9	25.4	10.2	63.6	11.0
2.2	25.4	5.7	26	10.8
1.7	24.5	4.4	24.7	10.1
1.7	25.4	4.9	22.4	11.9
2.2	25.4	5.5	11.7	14.9
2.2	25.4	5.5	37.7	8.4
6.0	18.6	11.6	37.7	9.5
6.4	16.9	11.3	22.4	10.7
4.7	16.9	8.3	16.5	11.1
5.2	16.1	8.6	25.9	12.1
5.6	16.1	9.3	28.3	10.4
			av	11.0 ± 0.9

$[C_2H_5Br]_0$[f]	laser fluence[c] (193 nm)	$[C_2H_5O_2]_0$[a,d]	[NO][d]	k_7[e]
4.8	3.4	5.7	17.7	9.6
4.8	3.0	5.2	16.6	13.9
1.8	9.5	6.2	30.6	8.2
2.3	9.5	7.7	25.3	13.4
1.9	9.5	6.5	23.6	10.0
2.3	9.5	7.8	21.1	11.3
			av	11.0 ± 2.5

[a] Estimated from the absorption cross section of the precursor and the laser fluence. [b] Units: 10^{14} molecules cm^{-3}. [c] Units: mJ cm^{-2} pulse^{-1}. [d] Units: 10^{12} molecules cm^{-3}. [e] Units: 10^{-12} cm^3 molecule^{-1} s^{-1}. [f] Units: 10^{15} molecules cm^{-3}.

$$C_2H_5O_2 + NO \rightarrow C_2H_5O + NO_2 \quad (7)$$

$$C_2H_5O + O_2 \rightarrow CH_3CHO + HO_2 \quad (16)$$

$$HO_2 + NO \rightarrow OH + NO_2 \quad (17)$$

Another suit of influential reactions was the production of CCl_3O_2 following the photolysis of CCl_4 and the consumption of a larger amount of NO by CCl_3O_2 than expected. A numerical simulation with $k_7 = (11.0 \pm 0.8) \times 10^{-12}$ (derived from C_2H_5I and C_2H_5Br experiments) well reproduces the experimental data for C_2H_6/CCl_4 as shown in Figure 6.

Possible Sources of Errors. Stated errors on the derived rate constants are above the 95% confidence interval. The major source of error is the uncertainty of the initial concentration of RO_2 radicals, arising from the uncertainties in the concentration of the precursor gas, the photolysis laser intensity, and the absorption cross section and the quantum yield. The relative errors were estimated to be 10%, 8%, and 5%, respectively. Therefore, the total error in the initial concentration of RO_2 is accumulated to approximately 16% which was included in the error estimation of rate constant derived by the second-order analysis for $C_2H_5O_2$ + NO. Another potential source of the errors is the overlap detection of side products. In the reaction of CH_3O_2 + NO, the isotopes of NO_2 ($^{15}NO_2$ or ^{17}ONO at *m*/*z* 47) overlap the target CH_3O_2 (*m*/*z* 47), and the side product HONO (*m*/*z* 47) also overlaps. The contribution of isotopic NO_2 at *m*/*z* 47 was estimated to be no more than 0.5% of the initial CH_3O_2 signal, using the NO_2 signal observed at *m*/*z* 46 and the natural isotope abundance. To check the possibility of HONO, acetone-d_6 was used as the radical precursor to generate CD_3O_2, and the signal of DONO was monitored at *m*/*z* 48 during the

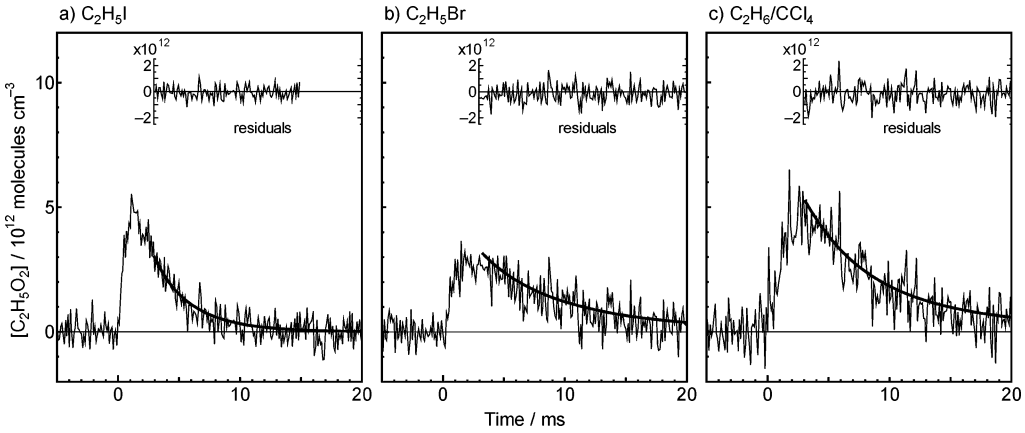

Figure 6. Comparison of the observed time profiles with kinetic simulations for $C_2H_5O_2 + NO$ experiments with the radical precursors (a) C_2H_5I, (b) C_2H_5Br, and (c) $C_2H_6 + CCl_4$: (a) $[C_2H_5O_2] = 1.0 \times 10^{13}$, $[NO] = 4.0 \times 10^{13}$, $[O_2] = 2.2 \times 10^{16}$; (b) $[C_2H_5O_2] = 5.7 \times 10^{12}$, $[NO] = 1.8 \times 10^{13}$, $[O_2] = 2.5 \times 10^{16}$; and (c) $[C_2H_5O_2] = 8.0 \times 10^{12}$, $[NO] = 3.8 \times 10^{13}$, $[O_2] = 2.2 \times 10^{16}$ molecules cm^{-3}. The rate constant for the target reaction was fixed to 11.0×10^{-12} cm^3 molecule^{-1} s^{-1} in the kinetic simulation. The ordinates are for kinetic simulations and the heights of experimental profiles were merely adjusted to match. Residuals were presented for the fitting range (a) 3−15, (b) 3−20, and (c) 3−20 ms.

TABLE 2: Comparison of Room Temperature Rate Constant Values for the $CH_3O_2 + NO$ Reaction and the $C_2H_5O_2 + NO$ Reaction

$CH_3O_2 + NO$		
ref	method[a]	k_6[f]
3	FP-KS	3.0 ± 1.7
4	MMS	6.5 ± 2.0
5	FP-UVA	7.1 ± 1.4
6	LP-LIF	8.1 ±1.6
7	FP-UVA	7.7 ± 0.9
8	DF-EIMS	8.6 ± 2.0
9	LP-LIF	7 ± 2
10	PR-UVA	8.8 ± 1.4
11	FT-CIMS	7.5 ± 1.3
12	LP-PIMS	11.2 ± 1.4
13	DF-EIMS	7.5 ± 1.0
14	TF-CIMS	7.8 ± 2.2
JPL[25] recommend value		7.7[b]
IUPAC[24] recommend value		7.7[c]
this work	LP-NIMS	9.9 ± 2.1
$C_2H_5O_2 + NO$		
ref	method[a]	k_7[f]
15	UVA	2.7 ± 0.2
10	PR-UVA	8.5 ± 1.2
16	FT-CIMS	9.3 ± 16
17	LP-IR/UVA	10.0 ± 1.5
18	FT-EIMS	8.9 ± 3.0
19	FT-CIMS	10.1 ± 0.9
20	DF-LIF	8.2 ± 1.6
JPL[25] recommend value		8.7[d]
IUPAC[24] recommend value		9.2[e]
this work	LP-NIMS	11.0 ± 0.9

[a] FP = flash photolysis, KS = kinetic spectroscopy, MMS = molecular modulation spectrometry, UVA = ultraviolet absorption, EIMS = electron impact mass spectrometry, LP = laser photolysis, LIF = laser-induced fluorescence, PR = pulse radiolysis, PIMS = photoionization mass spectrometry, CIMS = chemical ionization mass spectrometry, TF = turbulent flow, IR = infrared absorption. [b] Value is from a review by Tyndall et al.[30] in which the data in refs 6, 7, 11, 13, and 14 were used. [c] Value is the average of the values found in refs 6−8,11,13, and 14. [d] Value is obtained from the values in refs 10, 16−18, and 20. [e] Value is the average of the values in refs 10 and 16−20. [f] Units: 10^{-12} cm^3 molecule^{-1} s^{-1}.

reaction of CD_3O_2 with NO. No product at m/z 48 was discernible. It is not evident that any side products coincide with the mass number of $C_2H_5O_2$. No apparent signal was observed for CH_3ONO_2 or $C_2H_5ONO_2$.

Catalytic heterogeneous reactions on the reactor surface, such as NO ↔ NO(s) and RO_2 + NO(s) → products [where (s) denotes a molecule adsorbed on the reactor surface], may also be a source of error. Although no experiment was performed to assess this effect in the present study, the observed relatively small (∼3 s^{-1}) heterogeneous loss rate of RO_2 implies that the surface-catalyzed reaction is not likely to contribute significantly, compared to the radicals that indicate much larger wall loss rates (for example, the heterogeneous loss rate of OH radicals is 50∼150 s^{-1} in the similar Pyrex reactor without surface treatment).

Comparison with Previous Studies. As a summary, the present experimental study indicates the rate constants for reactions 6 and 7 to be $k_6 = (9.9 \pm 2.1) \times 10^{-12}$ and $k_7 = (11.0 \pm 0.8) \times 10^{-12}$ cm^3 molecule^{-1} s^{-1}, respectively. These are compared with the previous studies in Table 2. The present result for $CH_3O_2 + NO$ is 22−34% larger than the previous studies (data by Adachi and Basco[3] excluded), but is in good agreement with that of Masaki et al. Also the present result for $C_2H_5O_2 + NO$ is 8−25% larger than the previous reports (data by Adachi and Basco[15] excluded). Although the omission of the chain-regeneration of alkyl radicals in the experimental systems tends to result in the underestimation of the rate constants, no significant effect of this mechanism can be expected for many of the previous studies. The reasons for the discrepancy between the experimental results are not clear.

4. Conclusion

A new technique for the time-resolved detection of peroxy radicals has been developed. The reactions of methyl- and ethylperoxy radical with NO were studied experimentally with numerical kinetic analyses to verify the results. Several photolysis precursors were used for the generation of each peroxy radical to evaluate and eliminate the possible interference of the side reactions.

In the experiments for $CH_3O_2 + NO$ with acetone for the CH_3 source, and the experiments for $C_2H_5O_2 + NO$ with C_2H_6/CCl_4, the regeneration of the peroxy radicals by chain reactions was found to be significant. The rate constants were determined by the experiments with other precursors.

Either of the rate constants obtained in this study is about a factor of 1.3 larger than the previous recommendations.[24,25]

Acknowledgment. The authors thank Professor Nobuaki Washida at TUT (Toyohashi University of Technology) for his suggestion on the negative ionization method and useful comments and discussions on this study. Te authors also thank Professor Hiroyuki Matsui (TUT) for his continuous support and encouragement on the development of this new method. This work was supported in part by a Grant-in-Aid from the Ministry of Education, Science, Sports and Culture (No. 13640502 and priority field "Radical Chain Reactions").

References and Notes

(1) Atkinson, R. J. Phys. *Chem. Ref. Data* **1994**, Monograph No. 2.
(2) Carter, W. P. L.; Atkinson, R. *J. Atmos. Chem.* **1989**, *8*, 165.
(3) Adachi, H.; Basco, N. *Chem. Phys. Lett.* **1979**, *63*, 490.
(4) Cox, R. A.; Tyndall, G. S. *Chem. Phys. Lett.* **1979**, *65*, 35.
(5) Sander, S. P.; Watson, R. T. *J. Phys. Chem.* **1980**, *84*, 1664.
(6) Ravishankara, A. R.; Eisele, F. L.; Kreutter, N. M.; Wine, P. H. *J. Chem. Phys.* **1981**, *74*, 2267.
(7) Simonaitis, R.; Heicklen, J. *J. Phys. Chem.* **1981**, *85*, 2946.
(8) Plumb, I. C.; Ryan, K. R.; Steven, J. R.; Mulcahy, M. F. R. *J. Phys. Chem.* **1981**, *85*, 3136.
(9) Zellner, R.; Fritz, B.; Lorenz, K. *J. Atmos. Chem.* **1986**, *4*, 241.
(10) Sehested, J.; Nielson, O. J.; Wallington, T. J. *Chem. Phys. Lett.* **1993**, *213*, 457.
(11) Villalta, P. W.; Huey, L. G.; Howard, C. J. *J. Phys. Chem.* **1996**, *100*, 5808.
(12) Masaki, A.; Tsunashima, S.; Washida, N. *Chem. Phys. Lett.* **1994**, *218*, 523.
(13) Hellis, F.; Moortgat, G. K.; Crowley, J. N. *J. Phys. Chem.* **1996**, *100*, 17846.
(14) Scholtens, K. W.; Messer, B. M.; Cappa, C. D.; Elrod, M. J. *J. Phys. Chem. A* **1999**, *103*, 4378.
(15) Adachi, H.; Basco, N. *Chem. Phys. Lett.* **1979**, *64*, 431.
(16) Eberhard, J.; Howard, C. J. *Int. J. Chem. Kinet.* **1996**, *28*, 731.
(17) Maricq, M. M.; Szente, J. J. *J. Phys. Chem.* **1996**, *100*, 12374.
(18) Plumb, I. C.; Ryan, K. R.; Steven, J. R.; Mulcahy, M. F. R. *Int. J. Chem. Kinet.* **1982**, *14*, 183.
(19) Ranschaert, D. L.; J. Schneider, N. J.; Elrod, M. J. *J. Phys. Chem. A* **2000**, *104*, 5758.
(20) Däele, V.; Ray, A.; Vassalli, I.; Poulet, G.; Le Bras, G. *Int. J. Chem. Kinet.* **1995**, *27*, 1121.
(21) Kondow, T. *J. Phys. Chem.* **1987**, *91*, 1307.
(22) Lightfoot, P. D.; Kirwan, S. P.; Pilling, M. J. *J. Phys. Chem.* **1988**, *92*, 4938.
(23) Wang, B.; Hou, H.; Yoder, L. M.; Muckerman, J. M.; Fockenberg, C. *J. Phys. Chem. A* **2003**, *107*, 11414.
(24) Atkinson, R.; Baulch, D. L.; Cox, R. A.; Crowley, J. N.; Hampson, R. F.; Kerr, J. A.; Rossi, M. J.; Troe, J. *Summary of Evaluated Kinetic and Photochemical Data for Atmospheric Chemistry*; IUPAC, 2002. http://www.iupac-kinetic.ch.cam.ac.uk/.
(25) Sander, S. P.; Friedl, R. R.; Ravishankara, A. R.; Golden, D. M.; Kolb, C. E.; Kurylo, M. J.; Huie, R. E.; Orkin, V. L.; Molina, M. J.; Moortgat, G. K.; Finlayson-Pitts, B. J. *Chemical Kinetics and Photochemical Data for Use in Atmospheric Studies*; JPL Publication 02-25; Jet Propulsion Laboratory: Pasadena, CA, 2003.
(26) Rattigan, O. V.; Shallcross, D. E.; Cox, R. A. *J. Chem. Soc., Faraday Trans.* **1997**, *93*, 2839.
(27) Porret, D.; Goodeve, C. F. *Proc. R. Soc. London, Ser. A* **1938**, *165*, 31.
(28) Jung, K.-H.; Lee, C. M.; Yoo, H. S. *Can. J. Chem.* **1983**, *61*, 2486.
(29) Kee, R. J.; Rupley, F. M.; Miller, J. A. *Chemkin-II*, A Fortran Chemical Kinetics Package for the Analysis of Gas-Phase Chemical Kinetics: Sandia National Laboratories, 1986**;** Sandia Report SAND89-8009B UC-706.
(30) Tyndall, G. S.; Cox, R. A.; Granier, C.; Lesclaux, R.; Moortgat, G. K.; Pilling, M. J.; Ravishankara A. R.; Wallington, T. J. *J. Geophys. Res.* **2001**, *106*, 12157.